Linköping Studies in Science and Technology
Licentiate Thesis No. 1953

Epitaxy of oxide and nitride thin films grown by magnetron sputtering

Faezeh Alijan Farzad Lahiji

LINKÖPING UNIVERSITY

Linköping studies in science and technology
Licentiate Thesis No. 1953

Epitaxy of oxide and nitride thin films grown by magnetron sputtering

Faezeh Alijan Farzad Lahiji

Thin Film Physics Division
Department of Physics, Chemistry, and Biology (IFM)
Linköping University SE-581 83 Linköping, Sweden
Linköping 2023

ISBN 978-91-8075-018-9 (Tryckt)
ISBN 978-91-8075-019-6 (PDF)
https://doi.org/10.3384/9789180750196
ISSN 0280-7971

Abstract

The need for electronic devices with new functionalities has caused research to move in a way to design and utilize materials with high-performance thermoelectricity, widely used in batteries, sensors, and electronic devices. Two-dimensional materials (2D) with unique structures and remarkable properties have been identified to fabricate oxide heteroepitaxy. The growth of heteroepitaxy has been focused on the growth of high-quality films on single-crystalline substrates.

The preferred orientation and the crystallization of the materials with thin or two-dimensional structures require an understanding of epitaxy. In epitaxial growth, using a specific, well-defined substrate with lattice constants close to that film is decisive in controlling the film orientation with high epitaxial quality. The electrical, optical, magnetic, and structural properties of the film are strongly determined by the texture and its epitaxial alignment.
The majority of studies report epitaxial growth on Si and sapphire with different crystallographic orientations. The family of NaCl-structured materials covers a variety of nitrides and oxides broadly used in science and technology that have been epitaxially grown on monocrystalline Si and sapphire (Al_2O_3).

In this thesis, the structure and optical properties of NiO are investigated as functions of oxygen content on Si(100) and c-Al_2O_3 using pulsed dc reactive magnetron sputtering. It is found that NiO with cubic structure is a single phase with predominant orientation along (111) on both substrates. It is fiber textured on Si(100), while twin domain epitaxy is achieved on c-Al_2O_3. The growth of two cases of metal oxide and nitride films (NiO and CrN) with rock-salt (NaCl) structure is also demonstrated on r-plane sapphire. It is revealed that the NaCl-structured materials NiO and CrN grow with a tilted orientation relative to the substrate. This characterization and analysis of the epitaxy, crystallography, and growth modes yield a single and identical epitaxial relationship of these two cubic materials on r-plane sapphire, in contrast to earlier studies on NaCl-structured materials on r-plane sapphire, indicating several different orientation relationships. The results advance the understanding of growth modes and unusual epitaxial relationships of two cases of metal oxide and nitride films with rock-salt (NaCl) structure broadly used in science and technology on r-plane sapphire.

Preface

This licentiate thesis is part of my Ph.D. studies in the Energy Materials unit in the Thin Film Physics Division at the Department of Physics, Chemistry, and Biology (IFM), at Linköping University since September 2019.

This work was supported financially by the Swedish Government Strategic Research Area in Materials Science on Functional Materials at Linköping University (Faculty Grant SFO-Mat-LiU No. 2009 00971), the Knut and Alice Wallenberg foundation through the Wallenberg Academy Fellows program (KAW-2020.0196), the Swedish Research Council (VR) under Project No. 2021-03826, and the Swedish Energy Agency under project 46519-1.

I am enrolled in Agora Materiae, a multidisciplinary doctoral program at Linköping University supported by Swedish Government Strategic Research Area on Materials Science.

Faezeh Alijan Farzad Lahiji

Linköping 2023

Populävetenskaplig sammanfattning

Behovet av elektroniska komponenter med nya funktioner har fått forskningen att utvecklas på ett sätt för att designa och använda särskilda material med högpresterande termoelektricitet, som ofta används i batterier, sensorer och elektroniska enheter. Tvådimensionella material (2D) med unik struktur och anmärkningsvärda egenskaper har identifierats för hetereroepitaxi. Heteroepitaxi har fokuserats på tillväxten av högkvalitativa filmer på enkristallina substrat.

Den föredragna orienteringen och kristalliseringen av materialen med tunna eller tvådimensionella strukturer kräver förståelse för epitaxi. Vid epitaxiell tillväxt är användningen av specifikt väldefinierade substrat med gitterkonstanter nära filmens avgörande för att styra filmens orientering med hög epitaxiell kvalitet. De elektriska, optiska, magnetiska och strukturella egenskaperna hos filmen bestäms starkt av texturen och dess epitaxiella inriktning. De flesta studier rapporterar epitaxiell tillväxt på Si och safir med olika kristallografiska orienteringar. Familjen av NaCl-strukturerade material täcker en mängd olika nitrider och oxider som i stor utsträckning används inom vetenskap och teknik har odlats epitaxiellt på monokristallint Si och safir (Al_2O_3).

I denna avhandling undersöks NiO:s struktur och optiska egenskaper som funktioner av syrehalt på Si(100) och c-Al_2O_3 med hjälp av pulsad likströmsreaktiv magnetronsputtring. Kubisk NiO är ren med övervägande orientering längs (111) på båda substraten. Det är fibertexturerat på Si(100) medan tvillingdomänepitaxi uppnås på c-Al_2O_3. Tillväxten av två fall av metalloxid- och nitridfilmer (NiO och CrN) med stensaltstruktur (NaCl) demonstreras också på r-plan-safir. De NaCl-strukturerade materialen NiO och CrN växer med en lutande orientering i förhållande till substratet. Denna karakterisering och analys av epitaxi, kristallografi och tillväxtlägen ger ett enda och identiskt epitaxiellt förhållande för dessa två kubiska material på r-plan-safir, i motsats till tidigare studier på NaCl-strukturerade material på r-plan-safir där man observerat flera olika orienteringar. Resultaten främjar förståelsen av tillväxt och ovanliga epitaxiella samband för två två fall av metalloxid- och nitridfilmer med (NaCl) som används allmänt inom vetenskap och teknik

Included papers

Paper I

Growth and optical properties of NiO thin films deposited by pulsed dc reactive magnetron sputtering

Faezeh A. F. Lahiji [a], Samiran Bairagi [a], Roger Magnusson [a], Mauricio A. Sortica [b], Daniel Primetzhofer [b,c], Erik Ekström [a], Biplab Paul [a], Arnaud le Febvrier [a], Per Eklund [a]

[a] Thin Film Physics Division, Department of Physics, Chemistry and Biology, (IFM), Linköping University, SE-58183 Linköping, Sweden

[b] Tandem Laboratory, Uppsala University, Uppsala SE 75120, Sweden

[c] Division of Applied Nuclear Physics, Department of Physics and Astronomy, Uppsala University, Uppsala SE 75120, Sweden

Manuscript in final preparation

Contribution:

I was responsible for the planning of the work, selecting the material system, planning, and performing the film deposition. I performed most of the analysis and characterization and wrote the manuscript.

Paper II

Growth and unusual epitaxial relations of NiO and CrN thin films on r-Al_2O_3

Faezeh A. F. Lahiji, Biplab Paul, Arnaud le Febvrier, Per Eklund

Energy Materials Unit, Thin Film Physics Division, Department of Physics, Chemistry and Biology, (IFM), Linköping University, SE-58183 Linköping, Sweden

Submitted for publication

Contribution:

I planned, coordinated, and performed the depositions of NiO. I performed the characterization and was responsible for the crystallographic analysis and pole figures. I wrote the manuscript.

Acknowledgments

I would like to thank everyone who has helped, supported, and contributed to this work at ***Linköping University***, the ***Thin Film Physics Division***, and the ***Energy Materials Unit***.

In particular:

Per Eklund, my supervisor, for giving me a chance to pursue my passion. I am truly proud of being a part of your research group. I appreciate all your time and feedback on my work, presentations, and writing and for being so supportive.

Arnaud le Febvrier, my co-supervisor, I appreciate your patience, and insightful answers to all my questions, as well as for giving me the opportunity to learn and practice being creative and independent. Thank you for your informative way of teaching us Jessie, XRD, SEM, and much more. I'm excited to learn more from you in the future**.**

Biplab Paul, my co-supervisor, for your help, input, and support during my work planning and choosing the material system.

Marcus Ekholm, my mentor, for your input during the study plan meetings.

Rui Shu and ***Smita Gangaprasad Rao***, my office mates and friends, who have always helped with my experiments with Jessie and provided valuable feedback and discussions. ***Erik Ekström***, for your open discussion during meetings. ***Niraj Kumar Singh***, for all the nice time, experience, and discussions (science and life) in this office. All members, past and present, in the Energy Materials group, ***Clio Azina***, ***Binbin Xin***, ***Sathish Kumar Shanmugham***, ***Hairui Ma***, ***Victor Hjort***, ***Susmita Chowdhury, and Sanath Kumar Honnali***, thank you for your kind attitude.

Kenneth Järrendahl, for providing me with optical lab, ***Roger Magnusson,*** and ***Samiran Bairagi*** for all your valuable time, comments, and ideas to improve the ellipsometry model.

Daniel Primetzhofer and ***Mauricio Sortica*** for RBS measurement and analysis.

Thomas Lingefelt, ***Per Sandström***, ***Harri Savimäki***, thank you for your support during my training periods and help with my broken instruments in the labs and teaching times.

Ulf Frykman and ***Goran Rakic*** from IT department for all your technical and practical support.

All members of the Thin Film Physics and Materials Design Divisions (***Jens Birch***, ***Johanna Rosen***, ***Fredrik Eriksson***, ***Naureen Ghafoor***, ***Per Persson,*** and ***Grzegorz Greczynski***) for all your support, comments, and discussion during Monday's meeting, summer, and Christmas meetings.

Members of ***Agora Materiae***, ***Caroline Brommesson***, and the ***AFM*** conference for all the well-organized seminars.

I would like to thank ***Babak Bakhit***, ***Samira Dorri,*** and ***Alireza Farhadizadeh*** for discussing and giving me tips and scientific ideas on ongoing projects and the future.

My Iranian friends: ***Lida Khajavizadeh***, ***Fatemeh Rasti Boroojeni***, ***Sajjad Naeimipour,*** for helping me and having fun during the weekends.

All my friends in the Nanostructured Materials Division: ***Qurat Ul-Ain***, ***Maiara Moreno***, ***Janella Salamania***, ***Tun Wei Hsu***, ***Zhixing Wu***, and ***Nikolaos Giochalas***.

My dear parents deserve my special thanks for being supportive and encouraging me everywhere and anytime in all stages of my life. My brother and his family, ***Yasser***, ***Shiva***, and ***Arses***, and my sister and her husband, ***Shayesteh*** and ***Saleh,*** for always being there for me unconditionally.

Contents

1. Introduction

Many products in industry and society benefit from thin film technology. Thin films, with a thickness ranging from one atomic layer to several micrometers, can functionalize bulk materials to obtain or improve desired properties. Thin films are widely used in areas such as microelectronics, semiconductors, hard coatings, medical implants, and decorative coatings. For instance, microelectronics technology requires the integration of several thin films with different properties. Understanding the stability and the morphology of materials is a key factor in obtaining the right properties. Therefore, the orientation and crystallization have always been of great interest to control and improve the electrical, optical, magnetic, and structural properties of technological thin film devices. It is, therefore, essential to be able to control their structural and morphological properties. For example, the deposition method and process parameters, such as pressure or flow ratios of reactive gases in physical vapor deposition, all strongly influence the film morphology, orientation, roughness, and thickness [1–3].

Ceramic thin films, such as oxides and nitrides, are of great importance in hard coatings as well as electronic, magnetic, and thermal-management applications. Most oxides are generally insulating, while most transition-metal nitrides are metallic or semiconductors, which implies that these materials are of broad use as thin films in these application areas. The physical and chemical properties of oxide materials are strongly dependent on oxygen ions that influence the electronic properties as a result of different oxidation states [4]. Depending on the stoichiometry, the hardness and morphological properties change by a difference in electronic structure in transition metal nitride coatings [5]. Binary oxide and nitride materials with rock salt structure (NaCl), face-centered cubic $Fm\bar{3}m$ symmetry (Space group No.225), have a common structure and are frequently used in a wide range of applications. For instance, TiN and TaN have long been used in coating technology for cutting tools [6], diffusion barriers [7], or CaO and MgO are used as buffer or template layers in optical applications [8]. Control of preferential orientation in thin films can be achieved by epitaxial growth, i.e., growing a thin film with a well-defined crystallographic orientation relation to the underlying substrate, often a single crystal.

The present work is inspired by materials that have potential for use in increased energy efficiency in society, for example by harvesting waste heat. Nickel oxide (NiO), with NaCl type

structure, is useful for various applications such as batteries and sensors [9], it is a promising material for thermoelectric devices [10], and nonvolatile resistive random-access memory (RRAM) devices [11]. Single crystal CrN with NaCl-structure has been widely used in hard-coating and corrosion-resistant applications [12,13] and has more recently emerged as a promising material for thermoelectric energy harvesting. For the latter area of application, improving the thermoelectric properties has been a driver for research on band engineering in low dimensional materials [14,15], doping and changing the stoichiometry [16] and nanostructuring [17]. Thin or two-dimensional structures require understanding epitaxial growth, which plays an important role in achieving high carrier mobility and thermoelectric properties. High-quality epitaxial films are possible by employing specific well-defined substrates with lattice constants close to that of the film. This is a way to control the preferred orientation and crystallization of the film. The texture (preferred orientation) strongly affects the properties of the grown film, which can be orientation dependent. This emphasizes the need for investigating epitaxial growth of cubic materials, and systems such as perovskites, NaCl, fcc or bcc metals, transition metal oxides/nitrides and fluorite crystal structure (e.g., yttria-stabilized zirconia) systems have been studied for several decades [18]. Monocrystalline Si and sapphire (Al_2O_3) are widely used substrates for epitaxial growth.

The aim of the present work is to understand the effects of stoichiometry, substrate orientations, and growth parameters on the crystallographic orientation and optical properties of NiO and CrN thin films grown on Si, and sapphire (Al_2O_3) with c-plane and r-plane orientation.

2. Materials

Rock-salt (NaCl) structured materials, such as many binary nitrides or binary oxides, have $Fm\bar{3}m$ symmetry (space group No.225) and have a cell parameter typically ranging between a = 4.14 Å and a = 4.21 Å, shown in Figure. 2.1. The NaCl structure is ionic and consists of two fcc sublattices, with one metallic cation sublattice (Na, Al, Cu, Ni, Mg, Ti, Cr …) and an anionic sublattice (X = O, N, and Cl). The family of NaCl-structured materials covers a variety of nitrides and oxides (MgO, NiO, CrN, TiN) used for applications ranging from hard protective coating, diffusion barrier, optoelectronic, for energy harvesting devices, or as a buffer layer for epitaxial growth.

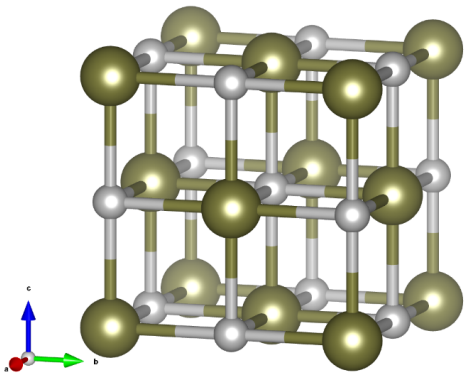

Figure. 2.1. NaCl structure, with two dissimilar atoms in face-centered cubic (FCC) lattices.

2.1. NiO

Nickel oxide (NiO), as a bulk material, has a cubic rock salt (NaCl) structure with octahedral Ni^{2+} and O^{2-} sites and a lattice parameter of 4.195 Å. It is a p-type semiconductor [19] with a wide band gap of 3.5-4 eV and high transparency in the visible region. NiO films often exhibit nonstoichiometry, meaning that the compositional ratio between nickel and oxygen deviates from one. The variation in stoichiometry changes the material characteristics and is useful for a wide range of applications. NiO has been studied for its magnetic [20], electronic [21], thermoelectric [16], and optical [22,23] properties as well as chemical resistance. NiO, as a p-type transparent conductor is a candidate for electrochromic devices such as inorganic smart windows [24]. It can be used as an antiferromagnetic layer [25] as well as for photovoltaics

[26], chemical sensors [27], and resistive random-access memories [28]. The properties of NiO thin films, like resistivity, electrical conductivity, and optical transparency, are strongly dependent on the type of deposition method [29], substrate temperature [30], and the amount of oxygen during the deposition [31]. In thin films, NiO with high crystallinity shows anisotropic crystallographic orientation due to the symmetry of the unit cell and their interatomic distance. NiO grown at a high substrate temperature typically consists of large grains with a coalesced structure, while a columnar structure is obtained at a lower substrate temperature. The epitaxial growth of NiO thin films and their preferred orientation strongly depend on the substrate. For instance, sapphire (Al_2O_3) monocrystalline substrate is one of the most commonly used ceramic materials for epitaxial growth of NiO thin film [32]. Two different phases of NiO, cubic NiO, and rhombohedral NiO are obtained on (Al_2O_3) (0001) substrates. The crystallinity of the film and the preferred orientation of NiO film can be controlled by the flowing gas species (O_2 and Ar) during the deposition [29]. The electrical conductivity of NiO is strongly affected by the presence of vacancies, which can be altered by oxygen flow ratio increment, which increases the hole concentration [33].

2.2. CrN

Chromium (Cr) is one of the transition metals belonging to group 6 in the periodic table, with low chemical stability compared to those of groups 4 and 5. Chromium nitride (CrN), with high mechanical hardness and good corrosion resistance, is an established material in industrial-scale applications for hard and corrosion-resistant coatings [34,35]. It has a low heat of nitride formation, and the hardness can be controlled by changing the nitrogen partial pressure [36]. Two crystal structures are common, the hexagonal structure Cr_2N (with a = 4.759 Å, c = 4.438 Å) [37] and CrN with NaCl (face-centered cubic, fcc) structure (with a = 4.149 Å) [38]. Also, CrN is highly stoichiometry dependent. N_2 partial pressure during the deposition can strongly affect its stoichiometry, morphology, and hardness [39]. The p-type and n-type Cr-based nitride materials are promising materials for thermoelectric devices [40–42]. Controlling the stoichiometry or doping is the key factor for transitioning between n-type and p-type or reverse for CrN films. The crystallinity and preferred orientation of CrN films are significantly affected by the types of substrates or the substrate temperature [43,44].

3. This Film Deposition and Growth

Thin film deposition is the transfer of atoms from a source (target) material to the location where the formation of film and growth are processed atomically (substrate). Deposition can be done by different techniques, such as physical vapor deposition (PVD), chemical vapor deposition (CVD), and hybrid methods (a combination of physical and chemical methods [45]). Chemical vapor deposition is based on the reaction of chemical gases with each other, usually at high temperatures, while physical vapor deposition is based on physical processes. The latter is a versatile class of techniques for thin-films and includes both evaporation and plasma-assisted sputtering. In PVD, the deposition source is a solid or liquid, which is transformed into a gas and/or plasma phase. Depending on the mechanism and type of transformation, PVD can be classified into thermal and electron beam evaporation, cathodic arc deposition, pulsed laser ablation, and different types of sputtering, such as ion beam sputtering or magnetron sputtering [46,47].

3.1. Sputtering

Sputtering is a physical process used for depositing materials in a high or ultrahigh vacuum environment by ejecting atoms from the surface of a solid or liquid cathode (known as a target) by bombardment with energetic particles. These particles are mainly noble gas ions, such as argon (Ar^+). The materials to be deposited are then condensed onto a substrate. The ejected atoms travel until they reach the substrate and condense on the substrate. They begin to form a film by binding to each other at a molecular level and finally forming a complete atomic layer. The number of atomic layers depends on the deposition rate and time.

Depending on the type of ions and their kinetic energy, various effects may occur in sputtering processes. The kinetic energy provided by ion bombardment plays an important role in sustaining the sputtering process. If the kinetic energy of ions transmitted to the target atoms is larger than their bonding energies, the bombarded atoms will be ejected. Generally, in addition to the ejected surface atoms, secondary electrons, reflected ions, and reflected noble-gas neutrals may also be emitted or backscattered from the target surface during sputtering [48]. The energy of the incoming ions defines the nature of the interaction with the surfaces. The incoming ions during the bombardment may be backscattered in collision with target atoms, some others implanted in the solid, transferring their energy to electrons and lattice atoms. They

may also diffuse further and become trapped in the solid, or they may be desorbed at the surface and buried beneath the surface layer [46]. The ion beam energy is explained by the interaction with the surface by changing the probability of the surface sticking and its reaction. The sticking probability as a function of the kinetic energy (eV), is defined by the ratio of the number of deposited atoms to the number of impinging ions at a kinetic energy less than 10^{-2} eV (or the thermal energy at room temperature), is unity. Thus, the ion sticking probability drops to about 0.2 eV at 20 eV in the range between 10^{-2} eV and 10^{4} eV. As soon as the kinetic energy increases, the sticking probability rises to 0.6 eV that the sputtering process occurs at this ion-energy range. The sticking probability rises to unity from 10^{4} eV and above up to 10^{6} eV when the ions are buried beneath the surface. Therefore, the sputtering probability is small in this range of energy.

I. Sputtering Yield

The efficiency of the sputtering process can be quantified by sputtering yield, which is the ratio between the number of ejected species and the number of ions bombarding the surface of a target. The sputtering yield depends on two main parameters: the energy of bombarding ions and the target material. In addition to ion energy, the angle of incident particles, mass, and charge of an ion, and, regarding the latter, the atomic number of elements, are essential parameters that determine the sputtering yield. Furthermore, the crystallinity and crystal orientation, as well as surface binding energy and mass of target atoms, play a critical role in sputtering yield [49]. For instance, sputtering yield increases with incident ion kinetic energy above 20 eV- 40 eV. For typical bombarding gases such as Ar, elements in the periodic table filled s shells such as Cu, Ag, and Au have the highest sputtering yields.

II. Origin of energetic particles

The initiation of sputtering is due to the bombardment of the target material with energetic ions. There are two common approaches to produce ions and induce sputtering of the target materials, ion guns, and plasma. For an ion gun, by placing an ion source facing the target, the required number of ions can be produced to enable sputtering and eventually the deposition of a thin film. Even though this technique is straightforward, it has limitations for large-scale and industrial applications. Using plasma as the source of ions can overcome these limitations. Plasma, as a highly efficient glow discharge ion source, can be operated using different types of low-cost gas such as hydrogen, nitrogen, and argon gas and is low gas consumption. The

optimum gas pressure to operate at is of the order of some millitorr; below ~1 mTorr the discharge becomes unstable. By applying a potential difference (high voltage) between two electrodes in the presence of a gas like argon (Ar) at low pressure, a continuous glow discharge originates the energetic particles (ions) that support the sputtering process. The ions gain energy in the electric field, and positively charged ions are attracted from the plasma toward the target. They bombard the target with sufficient energy to initiate sputtering.

III. Plasma

The term plasma was introduced by Irving Langmuir in 1928 [50]. Plasma is the fourth state of matter (the others being gas, liquid, and solid) and is defined as a collection of free-charged particles that is electrically neutral on average. By applying a sufficient voltage across two parallel conducting electrodes or plates immersed in a gaseous medium, the atoms and molecules of the medium will break down electrically and form electron-ion pairs to permit the current to flow.

Plasma, as a state of matter, is distinct from the other three. Generally, a solid can pass into a liquid at a high enough temperature and fixed pressure. By increasing the temperature, liquid transforms into a gas. At a sufficiently high temperature, the gas molecules decompose to form atoms. Free atoms move in a random direction and frequently collide with one another. If the temperature is further increased, the free atoms decompose into an equal number of positively and negatively charged particles. The charged particles are electrically neutral and can enter the plasma state.

The density of charged particles in the bulk plasma (negative and positive particles like positive ions and electrons) is equal and characterized by $n_e \approx n_i = n_0$ (n_0 denotes plasma density) particles/m^3 at equilibrium temperature $T_e = T_i = T$. That makes the plasma quasineutral, i.e., approximately electrically neutral when averaged over the entire plasma. The quasineutrality can be disturbed in the sheath, called the Debye sheath [51], between the plasma and the chamber wall, where the number of ions is greater than the electrons. In this configuration, due to the large mass difference between ions and electrons, the electrons move faster than ions and therefore leave the plasma to a greater extent. This results in the potential of the wall being negative relative to plasma. The process continues until a large enough potential difference between the plasma and the walls has been built up, resulting in a negative, repelling sheath drop. This makes the plasma potential positive relative to the walls. More electrons arriving

during sputtering will sustain the plasma due to secondary electron emission and ionization. Other objects inside the chamber, such as the substrate, which is not connected to the ground, acquire a negative potential in relation to the plasma potential. This makes electrons accumulate on the substrate surface due to the higher mobility of the electrons. This is known as "floating potential," which is due to the higher mobility of electrons.

3.1.1. Direct Current (dc) Sputtering

To generate plasma, a power source, like a direct current (dc) power supply, is needed to form a dc glow discharge. The chamber is pumped down to a base pressure, typically of the order of 1×10^{-4} Pa. A working gas such as Ar is introduced into the chamber. The introduced gas acts as a medium where the electrical discharge is initiated and sustained. By applying a few hundred volts to the cathode (the target), the voltage difference between the cathode and anode (substrate and chamber side walls) results in the formation of an electric field. Therefore, a very small current flows, and a visible glow discharge will appear between the cathode and anode. The free electrons that are created through atom ionization will be affected by the electric field and accelerate toward the anode.

Initially, the current is nearly constant because all of the charge is moving. As the voltage is increased, sufficient energy can be conveyed to the charged particles. Accelerated particles will gain energy to produce more charged particles. The charged particles will collide with neutral gas atoms, and ionization will occur as follows:

$$e^- + Ar \rightarrow 2e^- + Ar^+$$

The generated two electrons are ready to bombard two other neutrals. When Ar^+ ions accelerate and strike the cathode, a secondary electron is released [51]. High-energy secondary electrons produce more ions by collision with neutral gas atoms. These ions are accelerated back to the cathode and produce more electrons and more ions in turn. When the number of generated electrons is just sufficient to produce enough ions and again to regenerate the same number of electrons, this is when the discharge is self-sustaining. This cascade of ionizing collisions will ultimately result in the gas beginning to glow, the voltage dropping, and the current rising abruptly. This is called the "normal regime."

3.1.2. Radio Frequency (RF) Sputtering

While direct current sputtering is suitable for conductive target materials, radio frequency sputtering (RF) is used for the deposition of dielectric target materials or non-conductive insulating films [46,52] and coatings that can be used in semiconductors like oxides (AlO, SiO, and TaO). For DC sputtering of an insulating target, the glow discharge would not be stable due to the accumulation of positive charge on the target surface. In DC sputtering, the target and substrate function as anode and cathode and remain fixed during the sputtering process, in contrast to RF, in which the substrate and the target alternatingly act as the two electrodes, changing between the anode and cathode. An alternate current (AC) in the range of (power is used to form AC sputtering. By applying RF power at a high frequency, charges oscillate between two electrodes, and the electric field between the two electrodes changes alternatingly.

Therefore, during the positive half of the cycle, the electrons move toward the target, acting as a cathode (exhibiting a negative bias). On the negative half of the cycle, the target will be bombarded by the positive ions of discharge plasma, and the sputtered atoms will be deposited on the grounded substrate to form a film. Therefore, no more ions accelerate toward the substrate. Both electrodes gain a negative charge with respect to plasma. This results in sustaining the electric conductivity of electrodes during the deposition process. At low pressure, a high sputtering rate can be achieved. However, compared to DC sputtering, lower deposition rates, the high cost of power supplies, and the need for matching electrical networks are the drawbacks of RF sputtering. In addition to the above-mentioned complexity, nonuniform plasma density may result from nonuniform current density sputtering.

3.1.3. Magnetron Sputtering

The basic (diode) sputtering process is today of very limited interest in the deposition of thin films[1]. The diode sputtering technique suffers from its limitations of low sputtering deposition rate due to its low plasma density in front of the target. Since electrons travel straight into the gas and induce most of the ionization far from the target and only a few ions return to the target, this requires a high working pressure (>1 Pa) and a high discharge voltage (V_{dc} ~ 2-5 KV) which causes thermalization of the sputtered flux. Therefore, a higher ion current density

[1] Despite of the relative the main disadvantages of diode sputtering, including low deposition rates, high gas densities, and high discharge voltages, it can be used for magnetic materials.

(J_{dc} > ~ 1 mA/cm^2) with lower discharge voltage and lower working pressure is needed for the sputter-deposition technique to be commercially viable.

Planar magnetron sputtering discharge is a well-established technique for both metallic and dielectric material thin film deposition in both laboratory scale and industrial applications. In magnetron sputtering, introduced by Penning in the late 1930s [53], a magnetic field is used to confine the electrons in the vicinity of the sputtered cathode (target) to improve the efficiency of the sputtering. A magnetic field (B) can be formed by placing permanent magnets behind the target plate with different N and S poles. The polarity of the center magnet is different from the annular poles of magnets on the outer edge. That makes magnetic field lines go out from the edges and back into the center of the target, called conventional magnetron sputtering. The generated magnetic lines between the poles above the target surface prevent electrons from escaping the target. In magnetron sputtering, the trajectory of charged particles (e.g., electrons) is affected by both electric and magnetic fields. They are accelerated along the direction of the electric field while moving in a helical fashion, perpendicular to the magnetic field. The resulting motion of particles, the drift velocity, $U_{E/B}$, is perpendicular to both the E and the B vectors shown in Figure. 3.1.

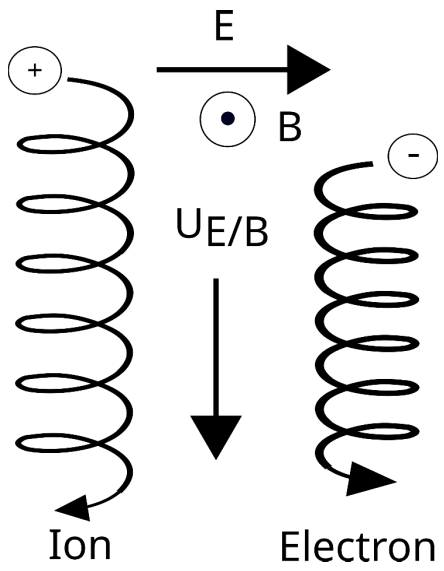

Figure. 3.1 Single particle motion in a combined electric and magnetic field. B points out of the plane of the paper. The figure adopted from F. F. Chen [54].

In this technique, plasma is confined in a magnetic field combined with an electric field. The configuration of magnets placed behind the target results in crossed E and B (E × B) fields, which generates a Hall drift of the electrons. The electron-velocity vector is parallel to the target surface, and the vertical component of the magnetic field, which is also parallel to the target, leads the electrons toward the central area between the two magnets. The magnetic fields significantly confine the movement of electrons and trap them in the target vicinity. Due to that, the chance of an ionizing collision probability with a gas atom increases. The results of increasing ionization efficiency led to increased ion bombardment and the creation of a racetrack on the target.

Consequently, the deposition rate will increase due to higher gas ionization. The process occurs when the cathode (target) is bombarded by highly energetic and unconfined Ar ions, resulting in the generation of a large number of secondary electrons. The way the electrons are accelerated back into the plasma, they are confined near the cathode by the magnetic field. Here, they undergo a sufficient number of ionizing collisions just to maintain the discharge before they are lost to the surface. The magnetron configuration behind the cathode can define the E×B drift path around the sputtered cathode. By confining the magnetic field, a dense plasma will be produced near the cathode while the substrate will be in an area with lower plasma density. Consequently, the substrate has a low ion current density due to bombardment by ions with low energy. That is a useful technique for heat-sensitive substrates, but it influences the microstructure and morphology of the film.

The energy of bombarding ions can be increased by providing a condition called an unbalanced magnetron sputtering configuration, developed by Window and Savvides in 1986 [55]. Figure. 3.2 is a schematic view of the magnetic design used in magnetron sputtering, where a typical magnet configuration in balanced magnetron sputtering (a) is compared versus unbalanced magnetron sputtering (b and c). In this configuration, the aim is to expand the discharge from the target and transport the plasma toward the substrate. By placing the magnets with the opposite polarity (to that in conventional magnetron sputtering), the produced magnetic fields above the target will be directed toward the substrate. This makes it possible to extract more ion current density from plasma and lead the secondary electrons to follow those magnetic field lines. Therefore, the dense plasma is not confined to the cathode target vicinity, but it can also extend toward the substrate. Consequently, the ion current density increases near the substrate, effectively influencing the deposition rate. The design of unbalanced magnetron

sputtering can be defined as type I and type II. In type I unbalanced magnetron sputtering, the central pole is strengthened relative to the outer poles, and all lines originate from the central magnets, some of those not passing into the annular magnets, directed toward the chamber wall. In type II, the outer rings of magnets are strengthened to the central pole, and the magnetic field lines originate from the annular magnets. While some of those do not pass into the central magnet and are directed toward the substrate, which is more commonly used. Controlling the magnetic field distribution above the target and having constant magnetron discharge of the target during the whole deposition time are the main advantages of using unbalanced magnetron sputtering.

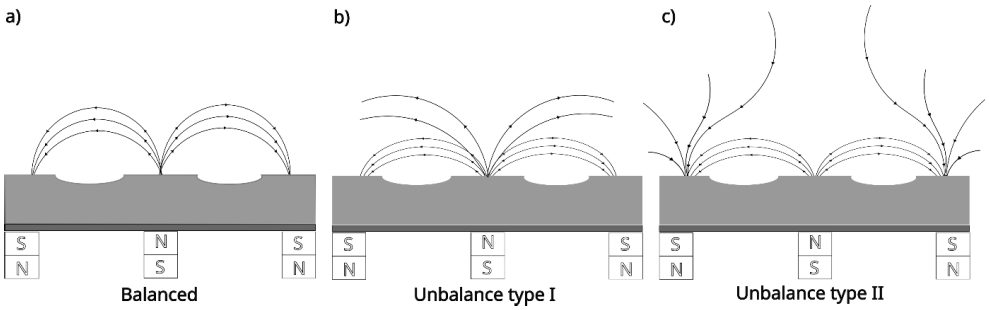

Figure. 3.2 Schematic view of the magnetic design used in magnetron sputtering: a) Balanced: all the filed lines originated from the central magnet and passed into the annular magnet, b) Unbalance type I: all the field lines originate from the central magnet, with some not passing into the annular magnet, c) Unbalance type II: all the field lines originate from the annular magnet, with some not passing into the cylindrical central magnet. The figure is adopted from Gudmundsson and Lundin (2020) [56].

3.1.4. Pulsed direct current magnetron sputtering

In pulsed dc magnetron sputtering, a pulsing unit is used with a combination of dc units to generate a pulsed dc voltage. It is an effective way to make thin films of different materials, from conductors to insulators, and basically materials that need a charge during the deposition. Pulsed dc sputtering is widely used in reactive sputtering, where an insulating layer is formed on the target material to eliminate the formation of an arc on the target surface. To discharge the built-up charge on the target, two common forms of unipolar and bipolar pulse sputtering.

In contrast to unipolar pulsed sputtering, where a positive voltage is applied to the power waveform to clean the target surface, bipolar pulsed sputtering uses two alternate pulses to apply to the target. Depending on the target material, the frequency range can be optimized from a couple of tens of kHz to 200 kHz. To reduce the dielectric accumulation, each magnet alternates between cathode and an anode. By applying the negative pulse of a few hundred volts

to the target, the sputtering will initiate, which is called “on time.” Then, at the end of this duty cycle, the voltage is reversed for a short time, which is called “reversed time,” with a positive charge to clean the target from the built-up charges. The reversed time is one-tenth of the time that the dielectric materials are charged on time and discharged during the reverse time.

3.1.5. Reactive magnetron sputtering

The process of sputtering in the presence of reactive gas is called reactive sputtering. In this process, the reactive gas reacts not only with deposited atoms on the substrate to form a compound but also with the surface atoms of the target. Therefore, the discharge parameters are affected due to changes in sputtering yield and yield of secondary electrons. High kinetic energy of ions can be formed by introducing the low-energy molecular or atomic (neutral) species of the reactive gas into the sputtering process. The ions with high energy can form a thick compound layer on the target surface. Therefore, the energy needed to break the compound layer's chemical bonds is higher than the energy of target metal atoms on the target. Therefore, the sputtering yield and deposition rate decrease when the poisoning process starts. Therefore, to maintain a metal surface on a target, a good amount of reactive gas is needed to obtain a compound film on the substrate and be able to sputter away the compound layer on the target surface. This is possible by controlling the partial pressure of reactive gas in relation to the total gas flow inserted into the chamber, in addition to placing the reactive gas flow near the substrate and directing Ar gas to the target [52].

3.2. Thin Film Growth

3.2.1. Epitaxy

Epitaxy is a term introduced by the French mineralogist L. Royer in 1928, consisting of two Greek words: “epi” meaning “placed or resting upon” and “taxis” meaning “arrangement on” [57]. The term "homoepitaxy" refers to the oriented growth of a crystalline material on the surface of another single crystal of a different (or occasionally the same) material. Under epitaxial growth, a particular plane of the crystal in the top layer meets the surface of the substrate such that the crystallographic direction of the top layer is parallel to some crystallographic direction in the substrate. This parallelism can be described by miller indices. The miller indices denote the crystallographic relations of the crystal planes and the direction between the top layer film and the underlying substrate. For instance, the epitaxial relationship

in a cubic-on-cubic system can be shown by $(001)[110] \parallel (001)[100](001)$ meaning that the (001) plane of the film is in contact with the same (001) plane of the substrate and the direction of the film coincides with the [100] direction of the substrate. In some cases, this epitaxial relationship may be at a non-zero angle, so that the film is rotated from the parallel orientation around the normal of the substrate surface. This provides a coincidence of high-index crystallographic direction with lower surface energy. Numerous modern devices, such as electronic, optoelectronic, and microelectronic devices, depend on the epitaxial growth of thin films. Two types of epitaxial films can be distinguished: homoepitaxy and heteroepitaxy. Homoepitaxy refers to the case when the crystal structure of the film and the substrate are identical with perfectly matched lattice paraments like Si on Si for the fabrication of integrated circuit transistors. Heteroepitaxy, which refers to the combination of two different materials having a similar crystal structure but a different lattice constant, like the deposition of crystalline cubic GaAs on a trigonal sapphire (Al_2O_3) substrate [58]. Microwave photonics and optoelectronic devices such as light-emitting diodes (LEDs) are based on heteroepitaxial growth.

4. Characterization of Thin Films

4.1. Structural Analysis and Morphology

4.1.1. X-ray-diffraction

X-ray diffraction (XRD) is a common and powerful technique for studying the crystal structure of materials. This technique is used for a wide variety of materials, ranging from single crystal epitaxial thin films to polycrystalline randomly oriented mixtures of powders and amorphous materials. Most materials are polycrystalline, i.e., made up of many small crystals. In a crystal, the repeating arrangement of atoms forms distinct planes separated by well-defined distances. When a sample is illuminated with a beam of X-rays, the atomic planes are exposed to the X-ray beam. Constructive interference can occur when the wavelength (λ) of X-rays is twice the distance (d) between atoms in a crystal. This can be determined by Bragg's law:

$$n\lambda = 2d_{hkl} \sin \theta \quad (4.1)$$

Here, d_{hkl} is the spacing between diffracting planes with the Miller indices hkl, θ is the angle between the sample and incident X-rays, λ is the X-ray wavelength, and n is an integer. A diffraction peak (constructive interference) is generated only if the angle (θ) between the incident beam and the crystallographic plane in the specimen fulfills Bragg's law. The principle of Bragg's law is illustrated in Figure. 4.1.

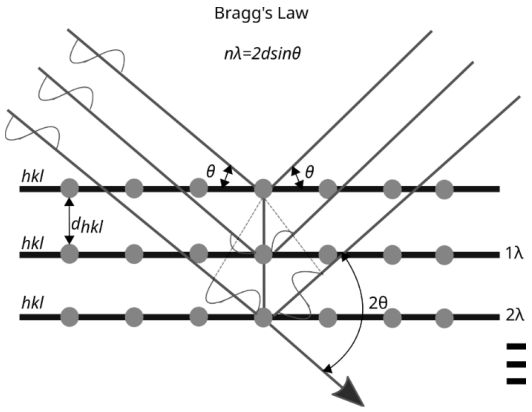

Figure. 4.1. Illustration of Bragg's law. The figure adopted from [59].

The θ-2θ Bragg-Brentano configuration is used in XRD measurements as the most common goniometer geometry with a fixed X-ray tube. In this geometry, the source and the detector are symmetric. The detector is adjusted to the same distance as the X-ray tube. Due to this arrangement, the sample is fixed in the center of a turning circle, and its surface is parallel to the diffracting plane. The sample is placed tangentially to the X-ray tube circle in the center of the goniometer.

4.1.2. Pole Figure

A pole figure measurement is employed to determine the crystal structure and orientation relationship of films. In this technique, the particular plane orientation is mapped with respect to the sample orientation. This is one way to investigate the crystallographic texture or preferred orientation of the sample. In this technique, the incident and diffracted beam angles, which are set to a specific plane spacing, are kept constant while the sample rotates and undergoes an azimuth angle of $\Phi = 360°$ along its normal. In this measurement, the scattering plane tilts from $\Psi = 0°$ to $\Psi = 85°$ continuously to give the stereographic projection of the plane orientation. The Ψ is called the tilt angle, which is the angle between the scatting plane vector (Q) and the normal of the sample. This information, taken from pole figure measurement, helps to investigate the epitaxial relationship between the film and the substrate.

4.1.3. Scanning Electron Microscopy

Scanning Electron Microscopy (SEM) is utilized for imaging metallic materials, ceramics, and semiconductors. It uses a focused beam of electrons to scan the surface of materials to image topography with high resolution and high magnification, along with compositional mapping. A variety of electrons can be produced as the electrons interact with the sample. These signals include backscattered electrons, secondary electrons, Auger electron characteristics, X-rays, and some others; each can be collected by specific detectors. The type of signal depends on acceleration voltage and the nature of the sample when the electron beam hits the surface. The secondary electron and backscattered electron are the most common signals that are produced and can be detected as a result of this interaction inside the sample. Backscattered electrons result from elastic interaction between the electron and the sample, which is reflected back from deep regions of the sample, with brighter contrast corresponding to higher atomic mass. Thus, a backscattered electron detector can provide both compositional and topographic imaging.

Secondary electrons originate from inelastic interactions between the electron beam and the sample. Due to its lower energy than the backscattered electron, it interacts with the sample surface or near-surface region. High-resolution morphological and topographical information are provided by two types of detectors in secondary electron signal: the In-Lens detector and the SE detector. The In-Lens detector takes advantage of being placed inside the electron column of the microscope right above the specimen to detect incoming secondary electrons with high efficiency. Due to electrostatic and magnetic field optimization, images with high lateral resolution can be obtained. In contrast, the SE detector gives better imaging of surface topography.

4.1.4. Spectroscopic Ellipsometry

Spectroscopic Ellipsometry (SE) is an optical technique that measures the change in the polarization state of light reflected from a material surface. This technique is mainly used for thin film, surface, and interface characterization. The optical properties of materials, such as refractive index or dielectric function, and the microstructural parameters like thickness, optical roughness, porosity, and crystal orientation, can be determined by spectroscopic ellipsometry. The change in polarization (ρ) of light depends on the surface and thin film properties and can be represented in a general procedure as follows. In principle, in any ellipsometry experiment, the objective is to measure the change in polarized light based on the light reflection on the plane of the sample or the light transmission through a sample. The polarization change is the difference between the detected information and the known input light, which is represented by $\Psi(\lambda)$ and $\Delta(\lambda)$. $\Psi(\lambda)$ represents the complex ratio of Fresnel reflection coefficients, r_p, when the polarized light is parallel to the plane of incidence and r_s, when the polarized light is perpendicular to the plane of incidence, and the phase difference between them is represented by $\Delta(\lambda)$.

A model must be constructed in order to relate the ellipsometric measurement parameter to the actual characteristics of the sample. The model, which is a physical description of the sample, is used to fit the model spectra to the experimentally derived $\Psi(\lambda)$ and $\Delta(\lambda)$ spectrum data. The model is described by its fit parameters, including the type of sample, the number of layers, the thickness, roughness, and optical properties of each layer. The model fit parameters are adjusted until the average of the difference between $\Psi(\lambda)$ and $\Delta(\lambda)$ spectra of the model is closely matched with the experimentally measured $\Psi(\lambda)$ and $\Delta(\lambda)$ spectra. In the fitting process, the

model closely approximates the real physical properties of the film. From model analysis, the thickness and roughness of the sample can be extracted with the addition of optical constants, complex refractive index or/and complex dielectric constant, and absorption coefficient. In the final step, the data analysis and the precision of the model are determined by a linear regression analysis given by the software. The mean squared error (MSE) evaluates the physical structure, and the lowest MSE reflects the true estimation of the thickness and optical constants. Even though there is the possibility to generate and simulate models for various unknown materials, data analysis is complicated because of different problems regarding the film structure, selection of appropriate model, isotropic and anisotropic, transparent, and absorption of materials. Therefore, it is necessary to have enough knowledge and information in advance about the optical constants of the material that is to be used for choosing the model with fewer parameters for fitting.

I. Definition of the ellipsometric parameters

Based on Maxwell's theory, light is a wave represented by two perpendicular vectors, the electric field (E) and the magnetic field (B), both perpendicular to the direction of light wave propagation. A beam of linearly polarized light incident on a surface changes the polarization state. Elliptically polarized light is produced when the light is reflected from the surface using a polarizer. As shown in Figure 4.2, the reflected light is decomposed into two components, parallel (E_p) and perpendicular (E_s) to the plane of incident light. After reflection, both the (E_p) parallel and (E_s) perpendicular components to the plane of incidence are out of phase, and the amplitude of the reflected light changes depending on the optical properties of the surface. Ellipsometry measures the phase difference (Δ) between E_p and E_s components and the change in the ratio of the amplitudes (Ψ).

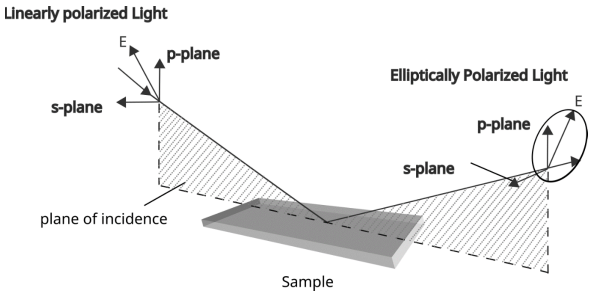

Figure. 4.2. Illustration of the principle of ellipsometry.

The resultant change in polarization after reflection from the surface can be measured by a complex reflection coefficient:

$$\rho = \tan(\psi)e^{j\Delta} = \rho(\varphi, \lambda, N_i, L_i) \tag{4.2}$$

where N_i and L_i are the complex indexes of refraction and thickness of the ith component and

$$tan\Psi = \frac{|r_p|}{|r_s|}, \quad \Delta = \delta_p - \delta_s \tag{4.3}$$

where δ_p and δ_s are the phase angles and where r_p and r_s are the Fresnel coefficients for the components p and s of light:

$$r_p = \frac{E_{rp}}{E_{ip}} = |r_p| \exp(i\delta_p) \tag{4.4}$$

$$r_s = \frac{E_{rs}}{E_{is}} = |r_s| \exp(i\delta_s) \tag{4.5}$$

The dielectric response function ε or pseudodielectric function <ε> is obtained directly from the measurement of ρ:

$$\langle\varepsilon\rangle = sin^2\varphi + sin^2\varphi tan^2\varphi \left(\frac{1-\rho}{1+\rho}\right)^2 \tag{4.6}$$

With

$$\varepsilon = \varepsilon_1 + i\varepsilon_2 \tag{4.7}$$

$$\varepsilon_1 = n^2 - k^2 \, , \varepsilon_2 = 2nk \tag{4.8}$$

where n and k are the real and imaginary parts of the complex index of refraction (N), which describes how light interacts with a given material, which is given as:

$$N = n - ik \tag{4.9}$$

The incident light at the boundary of two materials, some of the light reflects from the interface and some transmits. According to Snell's law, as shown in Figure. 4.3., the angle between the incident light and the normal of the sample (θ_i) is equal to the reflected angle, while the refracted angle, which is the angle between the normal of the sample and transmitted light (θ_t), is different based on the refractive index of new material.

$$n_i sin\theta_i = n_t sin\theta_t \tag{4.10}$$

Concurrently, as the light travels into a new material, the phase velocity of transmitted light can be described based on the new refractive index.

$$v = \frac{c}{n} \tag{4.11}$$

v is the speed of light in a material with a refractive index of n, and c is the speed of light in a vacuum.

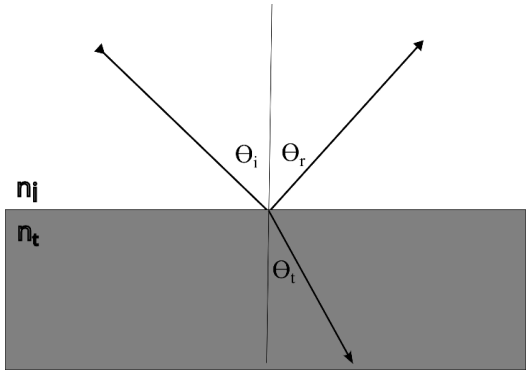

Figure. 4.3. Light reflection according to Snell's law.

The speed of light slows as it enters a material with a different index. The frequency of light remains constant while the wavelength shortens. The wavelength inside the material and the wavelength inside the material

$$\lambda_{mat} = \frac{2\pi c}{\omega n} = \frac{\lambda}{n} \tag{4.12}$$

The transmitted light also experiences absorption where the intensity of the light decreases corresponding to the distance (d) a wave travels into the medium. The absorption coefficient (α) can be calculated from the measured transmittance using Beer-Lamber's law:

$$I = I_0 e^{-\alpha d} \tag{4.13}$$

I and I_0 are transmitted and incident irradiance, where d is the path length for the light propagating through the material. The extinction coefficient describes the loss of wave energy to the material, which is proportional to the absorption coefficient:

$$\alpha = \frac{4\pi K}{\lambda} \tag{4.14}$$

II. Method

In this study, a Mueller matrix spectroscopic ellipsometer from J.A. Woollam Co, Inc. was used to measure samples over a spectral range of 210-1600 nm (0.7- 5.9 eV) at four angles of incidence from 45° to 75° in steps of 10°. CompleteEASE® modeling software from J.A. Woollam Co., Inc. (Lincoln, NE, U.S.A.), Version: 5.21, was used for the analysis and model fitting of acquired optical data. The optical properties, such as complex refractive index $N(\lambda) = n(\lambda) + ik(\lambda)$ (where n represents refractive index and k represents extinction coefficient) (or complex dielectric function) and absorption coefficient $\alpha(\lambda)$, were obtained from the model fitting of ellipsometric data, along with film thickness and surface roughness values.

To describe the optical constants, the Cauchy dispersion relationship (from J.A. Woollam Co., Inc. (Lincoln, NE, U.S.A.), Version: 5.21 library database) is applied as starting material in the transparent region. The Cauchy function is used to build the optical model for many materials at transparent wavelengths ($\varepsilon_2 \sim 0$).

The Cauchy model is used to model the normal dispersion of transparent materials in the visible region (~ 400 nm-800 nm) given as:

$$n(\lambda) = A + \frac{B}{\lambda^2} + \frac{C}{\lambda^4} \qquad , k(\lambda) = 0 \tag{4.15}$$

The coefficient (A) determines the amplitude of index n(λ), and B and C affect the curvature of the index n(λ) across the transparent wavelength. The B-spline parameterization is created by expanding the Cauchy (as the starting material in the transparent region) to the whole

wavelength and extending it into the absorbing region. A B-spline as a mathematical model is used to describe the dielectric function (complex structure in the absorption spectra (ε_2) and physically correct dispersion spectra (ε_2)), optical constant, and obtain an estimation of the thickness, roughness, and homogeneity of the film. The optical constants ε_1 and ε_2 are dependent on each other. Kramers–Kronig (K-K) consistency provides the relationship between ε_1 and ε_2. The optical constants of the bare Si substrate and single-sided polished c-Al_2O_3 were obtained using Si_JAW and a Tauc-Lorentz oscillator. Roughness and thickness play a significant role in the fitting process. Therefore, to generate optical constants during parametrization from Cauchy to B-spline, the thickness and roughness are free to have a low MSE error.

5. Main results and contribution to the field

This research is dedicated to the effect of oxygen flow ratio during deposition of NiO thin film on Si(100) and two different planes of sapphire, c- and r-Al_2O_3.

In **Paper I**, I investigate the effect of the stoichiometry of NiO thin films. The focus is on the effect of deposition conditions on the structure of NiO thin films grown on Si(100) and c-Al_2O_3 and the effect on optical properties. NiO thin films with varied oxygen content are grown on Si(100) and c-Al_2O_3 at a substrate temperature of 300 °C using pulsed dc reactive magnetron sputtering. The structure and optical properties of NiO change as functions of oxygen content. NiO with cubic structure, single phase, and predominant orientation along (111) is found on both substrates. X-ray diffraction and pole-figure analysis show that NiO on Si(100) substrate is fiber textured while twin domain epitaxy is achieved on c-Al_2O_3, with $NiO[111] \parallel Al_2O_3[0001]$ and $NiO[1\bar{1}0] \parallel Al_2O_3[10\bar{1}0]$ or $NiO[\bar{1}10] \parallel Al_2O_3[2\bar{1}\bar{1}0]$ epitaxial relationship. The refractive index and absorption coefficient of NiO films are affected by the oxygen content.

In **Paper II**, the epitaxial growth of NiO and CrN onto the r-Al_2O_3 substrate is compared and investigated. NiO and CrN are two NaCl structure materials used as a reference for the study of epitaxial growth on r-Al_2O_3. Epitaxial NiO and CrN thin films were grown on single crystal $Al_2O_3(1\bar{1}02)$ (r-plane sapphire) using magnetron sputtering. X-ray diffraction in ω-2θ configuration revealed that the NaCl-structured materials NiO and CrN grow with a tilted orientation relative to the substrate, with a tilt angle of relative to the substrate of $\omega = 16.9°$ determined from an in-depth pole-figure analysis of the NaCl-structured materials on r-plane sapphire. The full epitaxial relations can therefore be described as $(110)[\bar{2}2\bar{5}] \parallel (9\,\bar{9}\,0\,8)[11\bar{2}0]$, which contrasts with the more commonly observed $(100)[100]_{NaCl} \parallel (1\bar{1}02)[10\bar{1}0]_{Al_2O_3}$. These results are of general relevance for the growth of NaCl-structured cubic materials onto r-plane sapphire.

6. Outlook and future work

This licentiate thesis is focused on the epitaxial growth and properties of benchmark NaCl-structured materials onto sapphire and silicon substrates of different orientations, including unusual epitaxy on r-plane sapphire. Exploring this epitaxy for NiO-based materials and related oxides will be pursued in my future work. Furthermore, I aim to explore unconventional types of epitaxies, notably van der Waals epitaxy, a form of epitaxy that takes advantage of weak interaction as well as low interfacial energies of two-dimensional (2D) or layered materials that reduce the structural restrictions that are imposed by the single crystal substrate even under a large lattice mismatch [60].

There has been increasing interest in 2D and 2D layered materials (2DLMs) due to their multifunctionality for the next generation of flexible and transparent electronics for wearable, bendable, and stretchable electronic materials applications. They are materials with layered and planar structures consisting of two-dimensional layers. Along 2D directions, the atomic layers are formed by in-plane tight covalent or ionic bonds, while the same layers in out-of-plane direction are bonded by weak van der Waals interactions. These kinds of crystals can be cleaved easily along the layers, resulting in a chemically inert surface with no dangling bonds on the cleaved surface [61]. Due to the directional nature of epitaxial growth, the use of a single crystal substrate is a prerequisite to promote the arrangement of the adatom in the crystal film. Therefore, structural similarities such as crystal symmetry, lattice parameter, and thermal expansion coefficient between the substrate and the grown materials on top must be considered. On the contrary, van der Waals epitaxy takes advantage of weak interaction, reducing the structural restrictions and allowing growth even at a large lattice mismatch [60]. van der Waals epitaxy has the capability of preparing 2D layered materials onto other 2D layered materials such as MoO_3 [62], TiO_2, or ZnO [63] on muscovite mica ($KAl_2AlSi_3O_{10}(OH2)$) substrate or the growth of 3D crystal on a 2D layered substrate, NiO on muscovite mica substrate for instance [64]. Accordingly, graphene, with an atomically thin two-dimensional structure and mechanically flexible behavior, has been used as a platform to deposit high-quality oxide thin films and transfer them onto a flexible substrate [65]. On the other hand, the fabrication of van der Waals epitaxial growth of oxide materials directly on flexible substrates is challenging but would allow the fabrication of flexible 2D or free-standing 3D materials.

Particularly, transition metal oxides due to the strongly bonded structure as 3D materials cannot be readily formed into layers with a possibility of peeling off the top layer. By reducing the thickness from bulk to monolayer [66], electronic and thermoelectric properties may emerge. This can be expanded into multilayer structures consisting of two different materials grown alternately on top of each other with a controlled thickness at the nanometer scale to form a heterostructure that exhibits unique and remarkable electrical and optical attributes.

I aim to demonstrate the versatility of the van der Waals epitaxial growth for NiO, building on my previous work on conventional epitaxial growth in Paper I. NiO with a cubic rock-salt NaCl B1 structure consisting of two fcc sublattice, with one metallic cation sublattice (Me = Ni) and an anionic sublattice (O). The exfoliated mica substrate can be used to control the orientation of the NiO crystal during growth. The film can be transferred from the substrate to another substrate to form a free-standing thin film by implementing van der Waals epitaxial growth.

Furthermore, the same can be achieved for other oxides of two-dimensional layered materials (2DLMs), such as MO_x (M= V, Mo; x = 2, 3), but this poses additional challenges compared to NiO, which has a NaCl B1 cubic structure. Systems such as MO_x (and VO_2, shown by my colleague Erik Ekström [67], have multiple phases with different crystal structures (M1, M2, B, R, and A). This requires further research to grow the pure phase of VO_2 films with good crystal quality on 2D materials like muscovite (mica) to promote the further practical application of vdW heterostructures. Due to the van der Waals bond connection between the muscovite layers and its bendable, flexible, and light-weight structure, it is a great candidate for high-performance flexible optoelectronic devices. Muscovite is transparent and flexible in the micrometer range.

The heteroepitaxial growth of 3D oxide on 2D layered oxide with out-of-plane and in-plane epitaxial relationships can be obtained by the integration of VO_2 on muscovite [68] as $(010)_{VO_2}[200] \parallel [200](002)_{muscovite}$ or $(010)_{VO_2}[20\bar{2}] \parallel [200](002)_{muscovite}$ with the lattice parameter less than their bulk values. The structure variation of VO_2 is temperature dependent. The insulating monoclinic phase of VO_2 with P21/c space group reveals that at room temperature and with increasing temperature, the phonon intensities decrease, leading to transfer from monoclinic to metal phase with rutile structure [69].

To increase the functionality, a conducting layer is necessary for electrical contact in the deposition of epitaxially grown 3D oxide on 2D layered muscovite [70]. Band engineering is possible by applying varied interlayer spacing and tailoring the transition from direct to indirect bandgap [71]. MoO_2 with high conductivity can provide a suitable base layer for oxide heteroepitaxy. MoO_2 will grow epitaxially on muscovite due to the similar monoclinic structure with $< 010 >_{MoO_2} \| < 001 >_{muscovite}$ and $< 001 >_{MoO_2} \| < 100 >_{muscovite}$,an epitaxial relationship, and the lattice constant and d-spacing close to bulk, confirming no strain in the film.

To conclude, these strategies can be used for van der Waals epitaxy to tailor the growth of oxides, which I will pursue with the aim of property tailoring.

7. References

[1] I. Petrov, P.B. Barna, L. Hultman, J.E. Greene, Microstructural evolution during film growth, Journal of Vacuum Science & Technology A: Vacuum, Surfaces, and Films. 21 (2003) S117–S128. https://doi.org/10.1116/1.1601610.

[2] O. Lyandres, D. Finkelstein-Shapiro, P. Chakthranont, M. Graham, K.A. Gray, Preferred orientation in sputtered TiO 2 thin films and its effect on the photo-oxidation of acetaldehyde, Chemistry of Materials. 24 (2012) 3355–3362. https://doi.org/10.1021/cm301173j.

[3] Y. Wang, J. Ghanbaja, F. Soldera, S. Migot, P. Boulet, D. Horwat, F. Mücklich, J.F. Pierson, Tuning the structure and preferred orientation in reactively sputtered copper oxide thin films, Appl Surf Sci. 335 (2015) 85–91. https://doi.org/10.1016/j.apsusc.2015.02.028.

[4] K. Kalantar-zadeh, J.Z. Ou, T. Daeneke, A. Mitchell, T. Sasaki, M.S. Fuhrer, Two dimensional and layered transition metal oxides, Appl Mater Today. 5 (2016) 73–89. https://doi.org/10.1016/j.apmt.2016.09.012.

[5] P. Hones, N. Martin, M. Regula, F. Lévy, Structural and mechanical properties of chromium nitride, molybdenum nitride, and tungsten nitride thin films, J Phys D Appl Phys. 36 (2003) 1023–1029. https://doi.org/10.1088/0022-3727/36/8/313.

[6] J.E. Sundgren, Structure and properties of TiN coatings, Thin Solid Films. 128 (1985) 21–44. https://doi.org/10.1016/0040-6090(85)90333-5.

[7] C. Stampfl, A.J. Freeman, Stable and metastable structures of the multiphase tantalum nitride system, Phys Rev B Condens Matter Mater Phys. 71 (2005) 4–8. https://doi.org/10.1103/PhysRevB.71.024111.

[8] C.H. Lei, G. Van Tendeloo, J.G. Lisoni, M. Siegert, J. Schubert, Growth kinetic of MgO film on r-plane of sapphire: Microstructural study, J Cryst Growth. 226 (2001) 419–429. https://doi.org/10.1016/S0022-0248(01)01396-3.

[9] M.D. Irwin, D.B. Buchholz, A.W. Hains, R.P.H. Chang, T.J. Marks, p-Type semiconducting nickel oxide as an efficiency-enhancing anode interfacial layer in polymer bulk-heterojunction solar cells, Proc Natl Acad Sci U S A. 105 (2008) 2783–2787. https://doi.org/10.1073/pnas.0711990105.

[10] G. Parravano, P.S. Patil, L.D. Kadam, Preparation and characterization of spray pyrolyzed nickel oxide (NiO) thin films, J Chem Phys. 23 (2002) 211–221. https://doi.org/10.1016/S0169-4332(02)00839-5.

[11] H.Y. Peng, Y.F. Li, W.N. Lin, Y.Z. Wang, X.Y. Gao, T. Wu, Deterministic conversion between memory and threshold resistive switching via tuning the strong electron correlation, Sci Rep. 2 (2012) 1–6. https://doi.org/10.1038/srep00442.

[12] P. Hones, N. Martin, M. Regula, F. Lévy, Structural and mechanical properties of chromium nitride, molybdenum nitride, and tungsten nitride thin films, J Phys D Appl Phys. 36 (2003) 1023–1029. https://doi.org/10.1088/0022-3727/36/8/313.

[13] Y.L. Su, S.H. Yao, On the performance and application of CrN coating, Wear. 205 (1997) 112–119. https://doi.org/10.1016/S0043-1648(96)07286-9.

[14] Y. Pei, H. Wang, G.J. Snyder, Band engineering of thermoelectric materials, Advanced Materials. 24 (2012) 6125–6135. https://doi.org/10.1002/adma.201202919.

[15] Advanced Materials - 2007 - Dresselhaus - New Directions for Low-Dimensional Thermoelectric Materials.pdf, (n.d.).

[16] W. Shin, N. Murayama, High performance p-type thermoelectric oxide based on NiO, Mater Lett. 45 (2000) 302–306. https://doi.org/10.1016/S0167-577X(00)00122-1.

[17] P. Pichanusakorn, P. Bandaru, Nanostructured thermoelectrics, Materials Science and Engineering R: Reports. 67 (2010) 19–63. https://doi.org/10.1016/j.mser.2009.10.001.

[18] W. Seiler, M. Selmane, K. Abdelouhadi, J. Perrière, Epitaxial growth of gallium oxide films on c-cut sapphire substrate, Thin Solid Films. 589 (2015) 556–562. https://doi.org/10.1016/j.tsf.2015.06.034.

[19] P. Zhai, Q. Yi, J. Jian, H. Wang, P. Song, C. Dong, X. Lu, Y. Sun, J. Zhao, X. Dai, Y. Lou, H. Yang, G. Zou, Transparent p-type epitaxial thin films of nickel oxide, Chemical Communications. 50 (2014) 1854–1856. https://doi.org/10.1039/c3cc48877b.

[20] S. Ekeroth, S. Ikeda, R. Boyd, P. Münger, T. Shimizu, U. Helmersson, Impact of nanoparticle magnetization on the 3D formation of dual-phase Ni/NiO nanoparticle-based nanotrusses, Journal of Nanoparticle Research. 21 (2019) 1–9. https://doi.org/10.1007/s11051-019-4661-8.

[21] J.Y. Zhang, W.W. Li, R.L.Z. Hoye, J.L. MacManus-Driscoll, M. Budde, O. Bierwagen, L. Wang, Y. Du, M.J. Wahila, L.F.J. Piper, T.L. Lee, H.J. Edwards, V.R. Dhanak, K.H.L. Zhang, Electronic and transport properties of Li-doped NiO epitaxial thin films, J Mater Chem C Mater. 6 (2018) 2275–2282. https://doi.org/10.1039/c7tc05331b.

[22] B. Subramanian, M. Mohamed Ibrahim, V. Senthilkumar, K.R. Murali, V. Vidhya, C. Sanjeeviraja, M. Jayachandran, Optoelectronic and electrochemical properties of nickel oxide (NiO) films deposited by DC reactive magnetron sputtering, Physica B Condens Matter. 403 (2008) 4104–4110. https://doi.org/10.1016/j.physb.2008.08.014.

[23] M.A. Guziewicz, J.A. Grochowski, M.I. Borysiewicz, E.L. Kaminska, Electrical and optical properties of NiO films deposited by magnetron sputtering, XLI (2011) 1–10.

[24] G.A. Niklasson, C.G. Granqvist, Electrochromics for smart windows: Thin films of tungsten oxide and nickel oxide, and devices based on these, J Mater Chem. 17 (2007) 127–156. https://doi.org/10.1039/b612174h.

[25] E. Fujii, A. Tomozawa, H. Torii, R. Takayama, Preferred orientations of NiO films prepared by plasma-enhanced metalorganic chemical vapor deposition, Japanese Journal of Applied Physics, Part 2: Letters. 35 (1996). https://doi.org/10.1143/jjap.35.l328.

[26] H. Sato, T. Minami, S. Takata, T. Yamada, Transparent conducting p-type NiO thin films prepared by magnetron sputtering, Thin Solid Films. 236 (1993) 27–31. https://doi.org/10.1016/0040-6090(93)90636-4.

[27] I. Hotovy, V. Rehacek, P. Siciliano, S. Capone, L. Spiess, Sensing characteristics of NiO thin films as NO2 gas sensor, Thin Solid Films. 418 (2002) 9–15. https://doi.org/10.1016/S0040-6090(02)00579-5.

[28] X. Kang, J. Guo, Y. Gao, S. Ren, W. Chen, X. Zhao, NiO-based resistive memory devices with highly improved uniformity boosted by ionic liquid pre-treatment, Appl Surf Sci. 480 (2019) 57–62. https://doi.org/10.1016/j.apsusc.2019.02.216.

[29] H.W. Ryu, G.P. Choi, W.S. Lee, J.S. Park, Preferred orientations of NiO thin films prepared by RF magnetron sputtering, J Mater Sci. 39 (2004) 4375–4377. https://doi.org/10.1023/B:JMSC.0000033431.52659.e5.

[30] R.S. Kate, S.C. Bulakhe, R.J. Deokate, Effect of Substrate Temperature on Properties of Nickel Oxide (NiO) Thin Films by Spray Pyrolysis, J Electron Mater. 48 (2019) 3220–3228. https://doi.org/10.1007/s11664-019-07074-0.

[31] M. Wang, Y. Thimont, L. Presmanes, X. Diao, A. Barnabé, The effect of the oxygen ratio control of DC reactive magnetron sputtering on as-deposited non stoichiometric NiO thin films, Appl Surf Sci. 419 (2017) 795–801. https://doi.org/10.1016/j.apsusc.2017.05.095.

[32] J.H. Lee, Y.H. Kwon, B.H. Kong, J.Y. Lee, H.K. Cho, Biepitaxial growth of high-quality semiconducting NiO thin films on (0001) Al 2O 3 substrates: Microstructural characterization and electrical properties, Cryst Growth Des. 12 (2012) 2495–2500. https://doi.org/10.1021/cg3001174.

[33] Intrinsic states, 1 (1951).

[34] L. Swadźba, A. Maciejny, B. Formanek, P. Liberski, P. Podolski, B. Mendala, H. Gabriel, A. Poznańska, Influence of coatings obtained by PVD on the properties of aircraft compressor blades, Surf Coat Technol. 78 (1996) 137–143. https://doi.org/10.1016/0257-8972(94)02450-2.

[35] Y. Chiba, T. Omura, H. Ichimura, Wear resistance of arc ion-plated chromium nitride coatings, J Mater Res. 8 (1993) 1109–1115. https://doi.org/10.1557/JMR.1993.1109.

[36] V.M. Beresnev, O. V. Sobol', A.D. Pogrebnjak, S.S. Grankin, V.A. Stolbovoi, P. V. Turbin, A.A. Meilekhov, M.Y. Arseenko, Structure engineering in vacuum-arc-deposited coatings of the MoN–CrN system, Technical Physics Letters. 42 (2016) 532–535. https://doi.org/10.1134/S1063785016050205.

[37] M.F. Yan, H.T. Chen, Structural, elastic and electronic properties of Cr2N: A first-principles study, Comput Mater Sci. 88 (2014) 81–85. https://doi.org/10.1016/j.commatsci.2014.02.035.

[38] D. Gall, C.S. Shin, R.T. Haasch, I. Petrov, J.E. Greene, Band gap in epitaxial NaCl-structure CrN(001) layers, J Appl Phys. 91 (2002) 5882–5886. https://doi.org/10.1063/1.1466528.

[39] C. Rebholz, H. Ziegele, A. Leyland, A. Matthews, Structure, mechanical and tribological properties of nitrogen-containing chromium coatings prepared by reactive magnetron

sputtering, Surf Coat Technol. 115 (1999) 222–229. https://doi.org/10.1016/S0257-8972(99)00240-6.

[40] M.A. Gharavi, D. Gambino, A. le Febvrier, F. Eriksson, R. Armiento, B. Alling, P. Eklund, High thermoelectric power factor of pure and vanadium-alloyed chromium nitride thin films, Mater Today Commun. 28 (2021) 102493. https://doi.org/10.1016/j.mtcomm.2021.102493.

[41] A. Le Febvrier, N. Van Nong, G. Abadias, P. Eklund, P-type Al-doped Cr-deficient CrN thin films for thermoelectrics, Applied Physics Express. 11 (2018). https://doi.org/10.7567/APEX.11.051003.

[42] p-type behavior of CrN thin films via control of point defects.pdf, (n.d.).

[43] T. Elangovan, P. Kuppusami, R. Thirumurugesan, V. Ganesan, E. Mohandas, D. Mangalaraj, Nanostructured CrN thin films prepared by reactive pulsed DC magnetron sputtering, Mater Sci Eng B Solid State Mater Adv Technol. 167 (2010) 17–25. https://doi.org/10.1016/j.mseb.2010.01.021.

[44] Y.H. Liu, K. Wang, W. Lin, A. Chinchore, M. Shi, J. Pak, A.R. Smith, C. Constantin, The effect of growth parameters on CrN thin films grown by molecular beam epitaxy, Thin Solid Films. 520 (2011) 90–94. https://doi.org/10.1016/j.tsf.2011.06.052.

[45] W. Kern, J.L. Vossen, Thin film processes, Academic Press, 1978.

[46] M. Ohring, Materials science of thin films, Elsevier, 2001.

[47] J.O. Carlsson, P.M. Martin, Chemical vapor deposition Handbook of Deposition Technologies for Films and Coatings, Science, Technology and Applications. (2010) 444–445.

[48] D. Depla, S. Mahieu, others, Reactive sputter deposition, Springer, 2008.

[49] G. Greczynski, J. Lu, S. Bolz, W. Kölker, C. Schiffers, O. Lemmer, I. Petrov, J.E. Greene, L. Hultman, Novel strategy for low-temperature, high-rate growth of dense, hard, and stress-free refractory ceramic thin films, Journal of Vacuum Science & Technology A: Vacuum, Surfaces, and Films. 32 (2014) 041515. https://doi.org/10.1116/1.4884575.

[50] B.R. Adhikari, R. Khanal, Introduction to the Plasma State of Matter, Himalayan Physics. 4 (2013) 60–64. https://doi.org/10.3126/hj.v4i0.9430.

[51] M.A. Lieberman, A.J. Lichtenberg, Principles of plasma discharges and materials processing, John Wiley \& Sons, 2005.

[52] A.L. Gobbi, P.A.P. Nascente, D.C. Sputtering, in: Q.J. Wang, Y.-W. Chung (Eds.), Encyclopedia of Tribology, Springer US, Boston, MA, 2013: pp. 699–706. https://doi.org/10.1007/978-0-387-92897-5_1029.

[53] G. Bräuer, Magnetron Sputtering, Comprehensive Materials Processing. 4 (2014) 57–73. https://doi.org/10.1016/B978-0-08-096532-1.00403-9.

[54] F.F. Chen, others, Introduction to plasma physics and controlled fusion, Springer, 1984.

[55] N. Savvides, B. Window, Unbalanced magnetron ion-assisted deposition and property modification of thin films, Journal of Vacuum Science & Technology A: Vacuum, Surfaces, and Films. 4 (1986) 504–508. https://doi.org/10.1116/1.573869.

[56] J.T. Gudmundsson, D. Lundin, Introduction to magnetron sputtering, in: High Power Impulse Magnetron Sputtering: Fundamentals, Technologies, Challenges and Applications, Elsevier, 2019: pp. 1–48. https://doi.org/10.1016/B978-0-12-812454-3.00006-1.

[57] M. Ohring, S. Zarrabian, A. Grogan, The materials science of thin films, Appl Opt. 31 (1992) 7162.

[58] S.K. Saha, R. Kumar, A. Kuchuk, M.Z. Alavijeh, Y. Maidaniuk, Y.I. Mazur, S.Q. Yu, G.J. Salamo, Crystalline GaAs Thin Film Growth on a c-Plane Sapphire Substrate, Cryst Growth Des. 19 (2019) 5088–5096. https://doi.org/10.1021/acs.cgd.9b00448.

[59] D. Halliday, R. Resnick, J. Walker, Fundamentals of physics, John Wiley \& Sons, 2013.

[60] A. Koma, K. Yoshimura, Ultrasharp interfaces grown with Van der Waals epitaxy, Surf Sci. 174 (1986) 556–560. https://doi.org/10.1016/0039-6028(86)90471-1.

[61] A. Koma, Van der Waals epitaxy—a new epitaxial growth method for a highly lattice-mismatched system, Thin Solid Films. 216 (1992) 72–76.

[62] A.J. Molina-Mendoza, J.L. Lado, J.O. Island, M.A. Niño, L. Aballe, M. Foerster, F.Y. Bruno, A. López-Moreno, L. Vaquero-Garzon, H.S.J. Van Der Zant, G. Rubio-Bollinger, N. Agraït, E.M. Pérez, J. Fernández-Rossier, A. Castellanos-Gomez, Centimeter-Scale Synthesis of Ultrathin Layered MoO3 by van der Waals Epitaxy, Chemistry of Materials. 28 (2016) 4042–4051. https://doi.org/10.1021/acs.chemmater.6b01505.

[63] Y. Zhu, Y. Zhou, M.I. Bakti Utama, M.D. La Mata, Y. Zhao, Q. Zhang, B. Peng, C. Magen, J. Arbiol, Q. Xiong, Solution phase van der Waals epitaxy of ZnO wire arrays, Nanoscale. 5 (2013) 7242–7249. https://doi.org/10.1039/c3nr01984e.

[64] Y.H. Chu, Van der Waals oxide heteroepitaxy, NPJ Quantum Mater. 2 (2017) 1–5. https://doi.org/10.1038/s41535-017-0069-9.

[65] H. Kim, Y. Kim, K.S. Kim, H.Y. Jeong, A.R. Jang, S.H. Han, D.H. Yoon, K.S. Suh, H.S. Shin, T. Kim, W.S. Yang, Flexible thermochromic window based on hybridized VO2/graphene, ACS Nano. 7 (2013) 5769–5776. https://doi.org/10.1021/nn400358x.

[66] D. Ji, S. Cai, T.R. Paudel, H. Sun, C. Zhang, L. Han, Y. Wei, Y. Zang, M. Gu, Y. Zhang, W. Gao, H. Huyan, W. Guo, D. Wu, Z. Gu, E.Y. Tsymbal, P. Wang, Y. Nie, X. Pan, Freestanding crystalline oxide perovskites down to the monolayer limit, Nature. 570 (2019) 87–90. https://doi.org/10.1038/s41586-019-1255-7.

[67] scholar, E. Ekström, “Epitaxial Growth, Structure, and Thermoelectric Properties of CaMnand V-Based Oxides,” Thin Films Physics Division, Linköping University, 2021. (n.d.).

[68] C.I. Li, J.C. Lin, H.J. Liu, M.W. Chu, H.W. Chen, C.H. Ma, C.Y. Tsai, H.W. Huang, H.J. Lin, H.L. Liu, P.W. Chiu, Y.H. Chu, Van der Waal Epitaxy of Flexible and

Transparent VO2 Film on Muscovite, Chemistry of Materials. 28 (2016) 3914–3919. https://doi.org/10.1021/acs.chemmater.6b01180.

[69] R. Srivastava, L.L. Chase, Raman Spectrum of Semiconducting and Metallic VO, T 13 SRf s-I:MBFR 197I, n.d.

[70] C.H. Ma, J.C. Lin, H.J. Liu, T.H. Do, Y.M. Zhu, T.D. Ha, Q. Zhan, J.Y. Juang, Q. He, E. Arenholz, P.W. Chiu, Y.H. Chu, Van der Waals epitaxy of functional MoO 2 film on mica for flexible electronics, Appl Phys Lett. 108 (2016) 0–5. https://doi.org/10.1063/1.4954172.

[71] J. Li, W. Zhou, L. Xu, Y. Huang, S. Zhang, H. Zeng, Recent progress on the interfacial regulation and application of 2D antimonene-based van der Waals heterostructures, Appl Phys Lett. 121 (2022). https://doi.org/10.1063/5.0103000.

Papers

The papers associated with this thesis have been removed for copyright reasons. For more details about these see:

https://doi.org/10.3384/9789180750196

FACULTY OF SCIENCE AND ENGINEERING

Linköping Studies in Science and Technology, Licentiate Thesis No. 1953, 2023
Department of Physics, Chemistry, and Biology (IFM)

Linköping University
SE-581 83 Linköping, Sweden

www.liu.se